OPEN ACCESS

Original research

Craniosynostosis, inner ear, and renal anomalies in a child with complete loss of *SPRY1* (sprouty homolog 1) function

Rebecca S Tooze [1], Eduardo Calpena [1], Stephen R F Twigg [1], Felice D'Arco [2], The Genomics England Research Consortium, Emma L Wakeling [3], Andrew O M Wilkie [1]

ABSTRACT

Introduction *SPRY1* encodes protein sprouty homolog 1 (Spry-1), a negative regulator of receptor tyrosine kinase signalling. Null mutant mice display kidney/urinary tract abnormalities and altered size of the skull; complete loss-of-function of Spry-1 in humans has not been reported.

Methods Analysis of whole-genome sequencing data from individuals with craniosynostosis enrolled in the 100,000 Genomes Project identified a likely pathogenic variant within *SPRY1*. Reverse-transcriptase PCR and western blot analysis were used to investigate the effect of the variant on *SPRY1* mRNA and protein, in lymphoblastoid cell lines from the patient and both parents.

Results A nonsense variant in *SPRY1*, encoding p.(Leu27*), was confirmed to be heterozygous in the unaffected parents and homozygous in the child. The child's phenotype, which included sagittal craniosynostosis, subcutaneous cystic lesions overlying the lambdoid sutures, hearing loss associated with bilateral cochlear and vestibular dysplasia and a unilateral renal cyst, overlapped the features reported in *Spry1*$^{-/-}$ null mice. Functional studies supported escape from nonsense-mediated decay, but western blot analysis demonstrated complete absence of full-length protein in the affected child and a marked reduction in both parents.

Conclusion This is the first report of complete loss of Spry-1 function in humans, associated with abnormalities of the cranial sutures, inner ear, and kidneys.

WHAT IS ALREADY KNOWN ON THIS TOPIC

⇒ Loss of sprouty homolog 1 (Spry-1) function in the mouse causes defects in the kidneys and urinary tract, altered skull size, and other phenotypes, but the consequence of loss of the human orthologue has not been described.

WHAT THIS STUDY ADDS

⇒ We identifed a child homozygous for a nonsense variant affecting an N-terminal residue of *SPRY1*, causing complete loss of functional Spry-1 protein. The child's phenotype was notable for craniosynostosis and inner ear malformations, but only a minor renal abnormality. Neither parent exhibited evidence of related phenotypes.

HOW THIS STUDY MIGHT AFFECT RESEARCH, PRACTICE OR POLICY

⇒ These observations suggest a mouse-human species difference in the effects of Spry-1 deficiency and question previous reports suggesting that heterozygous loss of Spry-1 is pathological. Further observations are needed to corroborate these findings.

INTRODUCTION

Studies in *Drosophila* first identified sprouty as an important negative regulator of fibroblast growth factor receptor (FGFR) and other receptor tyrosine kinase (RTK) signalling pathways.[1] There are four mammalian sprouty homologues (encoded by *SPRY1-SPRY4*), that in humans range in size from 288 to 319 amino acids (aa), and share three regions of homology: a canonical Cbl-tyrosine kinase-binding domain (aa 51–57), a serine-rich domain (aa 112–131) and a cysteine-rich domain (aa 181–306; numbering refers to Spry-1, see online supplemental figure 1A).[2] Sprouty proteins lack enzymatic activity but decrease activation of the RAS-MAPK pathway, potentially by binding and sequestering the adapter protein GRB2 following sprouty phosphorylation by RTKs at key tyrosine residues, thus preventing membrane localisation of SOS, a RAS guanine exchange factor.[3]

Studies in mice have shown that homozygous deletion of the entire coding sequence of *Spry1* (orthologous to human *SPRY1*) affects multiple developmental processes; heterozygous mice (*Spry1*$^{+/-}$) are phenotypically normal. In the original report,[4] 95% of homozygous neonates (mixed genetic background) displayed unilateral or bilateral ureter and kidney malformations, and 71% died within 5 months. These abnormalities were principally attributable to loss of negative feedback regulation of the RET RTK in the Wolffian duct,[4] and could be phenocopied by homozygous substitution of the critical tyrosine residue (Tyr53Ala) within the Cbl-tyrosine kinase-binding domain.[4] Notably, crossing onto a different mouse strain background (FVB) was associated with reduced penetrance of urogenital malformations in *Spry1*$^{-/-}$ animals.[5]

► Additional supplemental material is published online only. To view, please visit the journal online (http://dx.doi.org/10.1136/jmg-2022-108946).

[1]Clinical Genetics Group, MRC Weatherall Institute of Molecular Medicine, University of Oxford, Oxford, UK
[2]Department of Radiology, Great Ormond Street Hospital for Children NHS Foundation Trust, London, UK
[3]North East Thames Regional Genetics Service, Great Ormond Street Hospital for Children NHS Foundation Trust, London, UK

Correspondence to
Prof Andrew O M Wilkie, MRC Weatherall Institute of Molecular Medicine, University of Oxford, Oxford, UK; andrew.wilkie@imm.ox.ac.uk

RST and EC contributed equally.

ELW and AOMW are joint senior authors.

Received 16 September 2022
Accepted 11 November 2022

Check for updates

To cite: Tooze RS, Calpena E, Twigg SRF, *et al*. *J Med Genet* Epub ahead of print: [please include Day Month Year]. doi:10.1136/jmg-2022-108946

Subsequently, detailed studies of *Spry1*$^{-/-}$ mice have revealed additional defects in multiple organs and cell types, including rostral cortex,[6] mammary gland,[7] mesenchymal stem cells[8] and muscle satellite cells.[9] These phenotypes are exacerbated by adding loss-of-function (LoF) alleles of other *Spry* genes (notably *Spry2*), indicating partial functional redundancy between Spry proteins.[10] Depending on strain background, both increased and decreased skull size were documented in *Spry1*$^{-/-}$ mice, but craniosynostosis was not reported.[11]

Bona fide disease-causing variants of human *SPRY1* have not been reported and therefore the consequence of complete LoF of the human orthologue was unknown. Here, we describe a homozygous *SPRY1* nonsense variant, identified in a patient with syndromic craniosynostosis. We show that this results in complete loss of Spry-1 and is also associated with severe defects of the inner ear and mild kidney abnormalities.

METHODS

Genetic investigation and variant filtering of whole-genome sequencing data

Following normal routine genetic investigations, the family was enrolled into the Genomics England 100,000 Genomes Project and Illumina whole-genome sequencing (WGS) was performed on the proband and both parents.[12] No clinically reportable variants were identified. The participant variant call format files were examined in the Genomics England Research Environment, as described.[13] Following annotation with Ensembl Variant Effect Predictor, the variants were filtered using a gnomAD (v.2.1.1) allele frequency of ≤0.01,[14] Combined Annotation Dependent Depletion (CADD) score ≥20 and no intersection with low complexity regions. Given the reported consanguinity, variants within homozygous regions identified using Illumina's ROHcaller were prioritised.

Functional analysis of cDNA and protein

Fresh blood was obtained from the proband and both parents to prepare genomic DNA and lymphoblastoid cell lines. Dideoxy-sequencing of genomic DNA was used to confirm the *SPRY1* variant. RNA was obtained from lymphoblastoid cells, following which *SPRY1* cDNA analysis (including deep sequencing) was performed by reverse transcriptase PCR (RT-PCR); protein was extracted for quantification of Spry-1 by western blotting. The antibody used to detect Spry-1 was rabbit mAb D9V6P (#13013, Cell Signaling Technology), detected using donkey anti-rabbit-horseradish peroxidase (HRP) (ab97085, abcam); anti-GAPDH-HRP (14C10, Cell Signaling Technology) was used as a loading control. Complete methods, including all primer sequences (online supplemental table 1) and PCR amplification conditions for genomic and cDNA analysis are provided in the online supplemental material.

Targeted resequencing of *SPRY1*

A search for additional variants in *SPRY1* was undertaken by targeted resequencing of 617 individuals with previously undiagnosed craniosynostosis (online supplemental methods and online supplemental table 2).

RESULTS

Case report

The index patient (II-1) is the first-born male child of consanguineous parents (half-first cousins; online supplemental figure 2A) of Indian descent. Apart from familial hypercholesterolaemia in the mother (I-2), both parents are healthy and phenotypically normal.

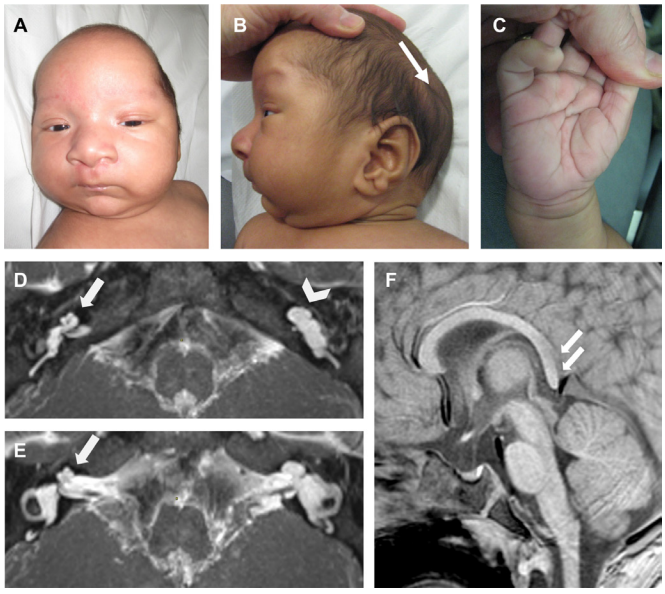

Figure 1 Clinical features of proband II-1 homozygous for *SPRY1* nonsense variant. (A–C) Photographs of the index patient aged 11 weeks showing scaphocephaly, turricephaly, bitemporal narrowing, hypertelorism, earlobe creases, cystic lesions overlying the lambdoid suture (B, arrow) and deep palmar crease (C). (D–F) Axial maximum intensity projection three-dimensional high-resolution T2-weighted images aged 8 months. (D–E) On his right side, he displays cochlear hypoplasia type 4 (arrows) with reasonably normal semi-circular canals. On the left, he has an incomplete partition type 1 cochlea (arrowhead), dilated vestibule with dysplastic lateral semi-circular canals. (F) Sagittal T1-weighted images showing small corpus callosum with hypoplastic splenium (double arrows).

Antenatal scans had shown increased nuchal translucency at 12 weeks and dolichocephaly from 20 weeks. Array comparative genomic hybridisation (aCGH) on an amniocentesis sample was normal. He was born at 39 weeks' gestation and noted at birth to have scaphocephaly, turricephaly, posterior ridging of the sagittal suture and bitemporal narrowing, with tense, symmetrically positioned cystic lesions (3×1 cm) over the parietal bones bilaterally. At 12 weeks of age, his length and weight were around the 50th centile; his head circumference could not be accurately measured owing to the cystic lesions. Distinctive facial features (figure 1A, 1B) included hypertelorism, a broad base to his nose, large ears with earlobe creases, and naevus flammeus over his philtrum and central forehead. There was a capillary malformation on his upper back. In his extremities, there was soft skin on his hands (figure 1C) with deep palmar and plantar creases, and a proximally placed overriding second toe on the right. CT scan of his head (aged 10 weeks) showed sagittal synostosis and bilateral subcutaneous cystic lesions over the lambdoid sutures. Aged 4 months, he had spring-assisted cranioplasty (removed at 8 months) and scalp lesions removed (shown histologically to be dermoid cysts).

He failed his newborn hearing screen and was subsequently found to have bilateral profound sensorineural hearing loss. MRI scan of his inner ear (aged 8 months) demonstrated bilateral inner ear dysplasia. On the right, there was cochlear hypoplasia with anterior off-set markedly hypoplastic apical turn (cochlear hypoplasia 4), similar to the unwound cochlea found in branchio-otorenal syndrome. The vestibule and semi-circular canals were relatively normal. On the left there was an incomplete partition

type 1 malformation of the cochlea with abnormal vestibule and semi-circular canals (figure 1D,E). The VIII nerves were normal bilaterally. He underwent bilateral cochlear implantation in a two-stage procedure (aged 15 and 18 months). MRI of the brain showed a small corpus callosum, which was dysmorphic posteriorly (figure 1F).

A renal ultrasound and renogram showed a simple left renal parapelvic cyst, while the right kidney appeared normal. He has normal renal function and is normotensive with no microalbuminuria; testes and external genitalia are normal. Echocardiogram at 3 months of age showed a small atrial septal defect (which had resolved spontaneously by 4 years) and mild supravalvular pulmonary stenosis of no clinical significance.

His speech and language development were delayed, consistent with his hearing loss. However, his motor and cognitive development is normal. At 4 years of age, he uses three-word sentences and follows complex instructions. Ophthalmology review was normal, with no concerns regarding his vision.

Molecular analysis

Initial genetic investigations of the proband included normal postnatal aCGH and craniosynostosis gene panel testing. Analysis of WGS data from the 100,000 Genomes Project showed that his genome harboured five regions of homozygosity ≥2 Mb (online supplemental figure 2B); after filtering three homozygous variants remained, including one stop-gain (in *SPRY1*) and two predicted missense variants (in *CCDC80* and *RASSF6*). Further evaluation of the *CCDC80* and *RASSF6* homozygous variants, as well as two heterozygous de novo missense variants (in *ATXN10* and *POMP*), did not support pathogenicity of these variants (online supplemental table 3), leaving the *SPRY1* variant as the sole candidate to be prioritised for further analysis. Dideoxy-sequencing confirmed the homozygous nonsense variant (c.80T>A, encoding p.(Leu27*) in *SPRY1*), which was heterozygous in both parents (figure 2A).

The premature termination codon, p.Leu27*, arises in the last and only coding exon of *SPRY1* (online supplemental figure 1A) and is therefore predicted to escape nonsense-mediated decay (NMD).[15] To confirm this, we undertook RT-PCR analysis of RNA extracted from lymphoblastoid cells and, in support, we identified RNA products in all three family members (figure 2B). The presence of the variant in the cDNA in approximately equal quantity to the normal allele was confirmed by deep sequencing of RT-PCR products from the parental samples, consistent with normal production of mutant RNA transcript and escape from NMD in lymphoblastoid cells (online supplemental table 4).

To assess the effect of the variant on Spry-1 protein synthesis, we undertook western blot analysis and identified a band of ~35 kDa in all healthy controls and both parents, corresponding to the expected size of Spry-1 (figure 2C). Of note, the antibody used was raised to an epitope comprising residues surrounding aa 70 of human Spry-1, located C-terminal of p.Leu27 (online supplemental figure 1A). Accordingly, the predicted truncated protein appeared entirely absent in the proband; band intensity was considerably weaker in both heterozygous parents compared with controls, consistent with loss of one copy of full length Spry-1. Results of replicate analyses and additional controls are shown in online supplemental figure 3.

DISCUSSION

To our knowledge, this is the first description of a patient harbouring a homozygous nonsense variant in *SPRY1*. This variant is predicted to affect all known *SPRY1* splice forms and to lead to a severely truncated Spry-1 protein that has lost all conserved features. The complete loss of full-length functional Spry-1 protein in the proband was corroborated by western blot analysis (figure 2C). The parents, who were phenotypically normal, were heterozygous for the variant and exhibited diminished amounts of full-length Spry-1 protein.

Major points of interest arising from this work are the delineation of human *SPRY1* LoF phenotypes in homozygous and heterozygous states, and comparison with the mouse null mutant. The patient shares many phenotypes previously reported in mouse *Spry1*$^{-/-}$ mutants (see 'Introduction' section), but with apparent differences in relative severity. Renal and ureteric anomalies, which are a major feature of the murine *Spry1*$^{-/-}$ phenotype and often lead to reduced viability, were manifested in the patient only as a unilateral simple parapelvic cyst, which did not compromise

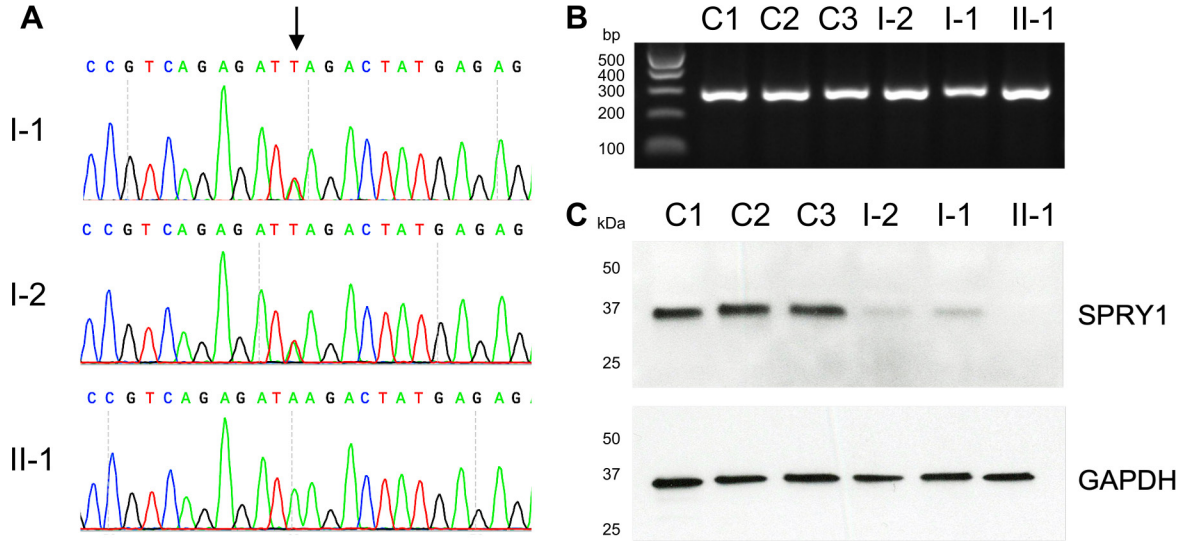

Figure 2 Identification of *SPRY1* nonsense variant and effect on expression of RNA and protein. (A) Dideoxy sequencing traces for each member of the pedigree. The arrow indicates the position of the c.80T>A nonsense variant in *SPRY1*. (B) RT-PCR of *SPRY1* including three unaffected controls (C1-3), the mother (I-2), father (I-1) and proband (II-1). (C) Western blot analysis using an antibody against Spry-1, targeting an epitope downstream of the stop-gain; lanes are labelled as in part B. The blots were stripped and reprobed using an antibody against GAPDH as a positive control.

renal function. By comparison, the patient exhibited major developmental abnormalities of the inner ear, affecting both the cochlea and vestibular systems; whereas inner ears of *Spry1*$^{-/-}$ mice are normal,[16] but manifest similar anatomical features when crossed with *Spry2* LoF alleles.[17] Given current evidence that the renal and inner ear abnormalities are predominantly driven by dysregulated signalling through different growth factor/RTK axes (GDNF/RET and FGF/FGFR, respectively), it is possible that these signalling pathways differ in their relative sensitivity to Spry-1 inhibition in the mouse and human. A failure to repress FGF/FGFR signalling is consistent with the presence of sagittal synostosis in the patient, since dysregulated FGF/FGFR signalling is a well-documented cause of this phenotype.[18] The patient manifested several additional phenotypes including dysmorphic facial features, bilateral dermoid cysts over the scalp and minor brain anomalies; the identification of additional cases is required to determine whether these fit into a consistent pattern.

We are aware of two previous reports of putatively pathogenic heterozygous *SPRY1* variants—a frameshift (p.(Gln6fs))[19] in a patient with sagittal synostosis, and a stop-gain (p.(Glu79*))[20] in a patient with Noonan syndrome (OMIM #609942). Two arguments suggest that these variants alone are unlikely to account for the associated phenotypes reported. First, the gnomAD dataset (v.2.1.1) identifies 13 individuals out of ~140 000 sequenced, including normal controls, heterozygous for LoF variants in *SPRY1*. This relatively high frequency conflicts with such alleles having highly penetrant pathogenic effects and accords with the low probability of LoF intolerance score (pLI=0). Second, in the current study, both parents were heterozygous for the LoF variant in *SPRY1* but displayed no relevant clinical phenotype. Importantly, no homozygous LoF variants are recorded in the gnomAD v.2.1.1 or v.3.1.1 datasets.

Based on similarities of the patient's phenotype with the mouse *Spry1*$^{-/-}$ mutant and absence of other credible pathogenic variants in the patient, we propose that complete loss of Spry-1 likely accounts for the abnormal phenotypes described. Further corroboration of genotype-phenotype correlations will require the identification of additional individuals harbouring homozygous variants in *SPRY1*; however, our attempts to identify such individuals through GeneMatcher, or by sequencing of 617 patients with unsolved craniosynostosis, were unsuccessful.

In conclusion, we present the first evidence of a *SPRY1* knockout in humans. Although these observations are based on a single case study, there are substantial overlaps with the reported phenotypes in *Spry1*$^{-/-}$ mutants in mice. Together with functional evidence showing loss of full-length protein within the proband, and lack of any other identified genetic pathology, we propose that the *SPRY1* variant is likely causative.

Twitter Rebecca S Tooze @becky_tooze

Acknowledgements We thank all the family members for their participation, the Genetics Lab at Great Ormond Street Hospital for support with obtaining samples and Dr Katherine Wood for advice on the deep sequencing experiment. This research was made possible through access to the data and findings generated by the 100,000 Genomes Project. The 100,000 Genomes Project is managed by Genomics England Limited (a wholly owned company of the Department of Health and Social Care). The 100,000 Genomes Project uses data provided by patients and collected by the National Health Service as part of their care and support.

Collaborators The Genomics England Research Consortium: JC Ambrose (Genomics England, London, UK); Arumugam, P. (Genomics England, London, UK); Bevers, R. (Genomics England, London, UK); Bleda, M. (Genomics England, London, UK); Boardman-Pretty, F. (Genomics England, London, UK; William Harvey Research Institute, Queen Mary University of London, London, UK); Boustred, C. R. (Genomics England, London, UK); Brittain, H. (Genomics England, London, UK); Brown, M.A. (Genomics England, London, UK); Caulfield, M. J. (Genomics England, London, UK; William Harvey Research Institute, Queen Mary University of London, London, UK); Chan, G. C. (Genomics England, London, UK); Giess A. (Genomics England, London, UK); Griffin, J. N. (Genomics England, London, UK); Hamblin, A. (Genomics England, London, UK); Henderson, S. (Genomics England, London, UK; William Harvey Research Institute, Queen Mary University of London, London, UK); Hubbard, T. J. P. (Genomics England, London, UK); Jackson, R. (Genomics England, London, UK); Jones, L. J. (Genomics England, London, UK; William Harvey Research Institute, Queen Mary University of London, London, UK); Kasperaviciute, D. (Genomics England, London, UK; William Harvey Research Institute, Queen Mary University of London, London, UK); Kayikci, M. (Genomics England, London, UK); Kousathanas, A. (Genomics England, London, UK); Lahnstein, L. (Genomics England, London, UK); Lakey, A. (Genomics England, London, UK); Leigh, S. E. A. (Genomics England, London, UK); Leong, I. U. S. (Genomics England, London, UK); Lopez, F. J. (Genomics England, London, UK); Maleady-Crowe, F. (Genomics England, London, UK); McEntagart, M. (Genomics England, London, UK); Minneci F. (Genomics England, London, UK); Mitchell, J. (Genomics England, London, UK); Moutsianas, L. (Genomics England, London, UK; William Harvey Research Institute, Queen Mary University of London, London, UK); Mueller, M. (Genomics England, London, UK; William Harvey Research Institute, Queen Mary University of London, London, UK); Murugaesu, N. (Genomics England, London, UK); Need, A. C. (Genomics England, London, UK; William Harvey Research Institute, Queen Mary University of London, London, UK); O'Donovan P. (Genomics England, London, UK); Odhams, C. A. (Genomics England, London, UK); Patch, C. (Genomics England, London, UK; William Harvey Research Institute, Queen Mary University of London, London, UK); Perez-Gil, D. (Genomics England, London, UK); Pereira, M. B. (Genomics England, London, UK); Pullinger, J. (Genomics England, London, UK); Rahim, T. (Genomics England, London, UK); Rendon, A. (Genomics England, London, UK); Rogers, T. (Genomics England, London, UK); Savage, K. (Genomics England, London, UK); Sawant, K. (Genomics England, London, UK); Scott, R. H. (Genomics England, London, UK); Siddiq, A. (Genomics England, London, UK); Sieghart, A. (Genomics England, London, UK); Smith, S. C. (Genomics England, London, UK); Sosinsky, A. (Genomics England, London, UK; William Harvey Research Institute, Queen Mary University of London, London, UK); Stuckey, A. (Genomics England, London, UK); Tanguy M. (Genomics England, London, UK); Taylor Tavares, A. L. (Genomics England, London, UK); Thomas, E. R. A. (Genomics England, London, UK; William Harvey Research Institute, Queen Mary University of London, London, UK); Thompson, S. R. (Genomics England, London, UK); Tucci, A. (Genomics England, London, UK; William Harvey Research Institute, Queen Mary University of London, London, UK); Welland, M. J. (Genomics England, London, UK); Williams, E. (Genomics England, London, UK); Witkowska, K. (Genomics England, London, UK; William Harvey Research Institute, Queen Mary University of London, London, UK); Wood, S. M. (Genomics England, London, UK; William Harvey Research Institute, Queen Mary University of London, London, UK); Zarowiecki, M. (Genomics England, London, UK).

Contributors Patient recruitment and assessment: FD'A, ELW. Data curation: RST, EC, The Genomics England Research Consortium. Formal analysis: RST, EC, SRFT, AOMW. Funding acquisition: SRFT, AOMW. Investigation: RST, EC. Supervision: SRFT, AOMW. Writing—original draft: RST, FD'A, ELW, AOMW. Writing—review and editing: all authors. AOMW is the guarantor of the final content of the paper.

Funding This work was supported by a Doctoral Training Programme studentship funded jointly by the Radcliffe Department of Medicine, Exeter College (Oxford) Usher Cunningham Scholarship and the MRC (RST), the NIHR Oxford Biomedical Research Centre Programme (AOMW) and the WIMM Strategic Alliance (G0902418 and MC UU 12025), the VTCT Foundation (SRFT, AOMW) and the MRC through a Project Grant MR/T031670/1 (AOMW). The 100,000 Genomes Project is funded by the National Institute for Health Research and NHS England. The Wellcome Trust, Cancer Research UK and the Medical Research Council have also funded research infrastructure.

Competing interests None declared.

Patient consent for publication Consent obtained from parent(s)/guardian(s).

Ethics approval The clinical protocol for 100,000 Genomes Project was approved by East of England—Cambridge South Research Ethics Committee (REC) (14/EE/1112). Experimental studies were performed under the protocol for Genetic Basis of Craniofacial Malformations (London—Riverside REC (09/H0706/20)). Written consent was obtained for both studies. Participants gave informed consent to participate in the study before taking part.

Provenance and peer review Not commissioned; externally peer reviewed.

Data availability statement All data relevant to the study are included in the article.

ORCID iDs
Rebecca S Tooze http://orcid.org/0000-0003-1396-3765
Eduardo Calpena http://orcid.org/0000-0001-6399-6528
Stephen R F Twigg http://orcid.org/0000-0001-5024-049X
Felice D'Arco http://orcid.org/0000-0001-7396-591X
Emma L Wakeling http://orcid.org/0000-0001-5712-0044
Andrew O M Wilkie http://orcid.org/0000-0002-2972-5481

REFERENCES

1 Hacohen N, Kramer S, Sutherland D, Hiromi Y, Krasnow MA. Sprouty encodes a novel antagonist of FGF signaling that patterns apical branching of the Drosophila airways. *Cell* 1998;92:253–63.
2 Guy GR, Jackson RA, Yusoff P, Chow SY. Sprouty proteins: modified modulators, matchmakers or missing links? *J Endocrinol* 2009;203:191–202.
3 Lorenzo C, McCormick F. SPRED proteins and their roles in signal transduction, development, and malignancy. *Genes Dev* 2020;34:1410–21.
4 Basson MA, Akbulut S, Watson-Johnson J, Simon R, Carroll TJ, Shakya R, Gross I, Martin GR, Lufkin T, McMahon AP, Wilson PD, Costantini FD, Mason IJ, Licht JD. Sprouty1 is a critical regulator of GDNF/RET-mediated kidney induction. *Dev Cell* 2005;8:229–39.
5 Yang X, Pande S, Koza RA, Friesel R. Sprouty1 regulates gonadal white adipose tissue growth through a PDGFRalpha/beta-Akt pathway. *Adipocyte* 2021;10:574–86.
6 Faedo A, Borello U, Rubenstein JLR. Repression of Fgf signaling by sprouty1-2 regulates cortical patterning in two distinct regions and times. *J Neurosci* 2010;30:4015–23.
7 Koledova Z, Zhang X, Streuli C, Clarke RB, Klein OD, Werb Z, Lu P. *SPRY1* regulates mammary epithelial morphogenesis by modulating EGFR-dependent stromal paracrine signaling and ECM remodeling. *Proc Natl Acad Sci U S A* 2016;113:E5731–40.
8 Urs S, Venkatesh D, Tang Y, Henderson T, Yang X, Friesel RE, Rosen CJ, Liaw L. Sprouty1 is a critical regulatory switch of mesenchymal stem cell lineage allocation. *Faseb J* 2010;24:3264–73.
9 Shea KL, Xiang W, LaPorta VS, Licht JD, Keller C, Basson MA, Brack AS. Sprouty1 regulates reversible quiescence of a self-renewing adult muscle stem cell pool during regeneration. *Cell Stem Cell* 2010;6:117–29.
10 Ching ST, Cunha GR, Baskin LS, Basson MA, Klein OD. Coordinated activity of Spry1 and Spry2 is required for normal development of the external genitalia. *Dev Biol* 2014;386:1–11.
11 Percival CJ, Marangoni P, Tapaltsyan V, Klein O, Hallgrímsson B. The interaction of genetic background and mutational effects in regulation of mouse craniofacial shape. *G3* 2017;7:1439–50.
12 Smedley D, Smith KR, Martin A, Thomas EA, McDonagh EM, Cipriani V, Ellingford JM, Arno G, Tucci A, Vandrovcova J, Chan G, Williams HJ, Ratnaike T, Wei W, Stirrups K, Ibanez K, Moutsianas L, Wielscher M, Need A, Barnes MR, Vestito L, Buchanan J, Wordsworth S, Ashford S, Rehmström K, Li E, Fuller G, Twiss P, Spasic-Boskovic O, Halsall S, Floto RA, Poole K, Wagner A, Mehta SG, Gurnell M, Burrows N, James R, Penkett C, Dewhurst E, Gräf S, Mapeta R, Kasanicki M, Haworth A, Savage H, Babcock M, Reese MG, Bale M, Baple E, Boustred C, Brittain H, de Burca A, Bleda M, Devereau A, Halai D, Haraldsdottir E, Hyder Z, Kasperaviciute D, Patch C, Polychronopoulos D, Matchan A, Sultana R, Ryten M, Tavares ALT, Tregidgo C, Turnbull C, Welland M, Wood S, Snow C, Williams E, Leigh S, Foulger RE, Daugherty LC, Niblock O, Leong IUS, Wright CF, Davies J, Crichton C, Welch J, Woods K, Abulhoul L, Aurora P, Bockenhauer D, Broomfield A, Cleary MA, Lam T, Dattani M, Footitt E, Ganesan V, Grunewald S, Compeyrot-Lacassagne S, Muntoni F, Pilkington C, Quinlivan R, Thapar N, Wallis C, Wedderburn LR, Worth A, Bueser T, Compton C, Deshpande C, Fassihi H, Haque E, Izatt L, Josifova D, Mohammed S, Robert L, Rose S, Ruddy D, Sarkany R, Say G, Shaw AC, Wolejko A, Habib B, Burns G, Hunter S, Grocock RJ, Humphray SJ, Robinson PN, Haendel M, Simpson MA, Banka S, Clayton-Smith J, Douzgou S, Hall G, Thomas HB, O'Keefe RT, Michaelides M, Moore AT, Malka S, Pontikos N, Browning AC, Straub V, Gorman GS, Horvath R, Quinton R, Schaefer AM, Yu-Wai-Man P, Turnbull DM, McFarland R, Taylor RW, O'Connor E, Yip J, Newland K, Morris HR, Polke J, Wood NW, Campbell C, Camps C, Gibson K, Koelling N, Lester T, Németh AH, Palles C, Patel S, Roy NBA, Sen A, Taylor J, Cacheiro P, Jacobsen JO, Seaby EG, Davison V, Chitty L, Douglas A, Naresh K, McMullan D, Ellard S, Temple IK, Mumford AD, Wilson G, Beales P, Bitner-Glindzicz M, Black G, Bradley JR, Brennan P, Burn J, Chinnery PF, Elliott P, Flinter F, Houlden H, Irving M, Newman W, Rahman S, Sayer JA, Taylor JC, Webster AR, Wilkie AOM, Ouwehand WH, Raymond FL, Chisholm J, Hill S, Bentley D, Scott RH, Fowler T, Rendon A, Caulfield M, 100,000 Genomes Project Pilot Investigators. 100,000 Genomes Pilot on Rare-Disease Diagnosis in Health Care - Preliminary Report. *N Engl J Med* 2021;385:1868–80.
13 Hyder Z, Calpena E, Pei Y, Tooze RS, Brittain H, Twigg SRF, Cilliers D, Morton JEV, McCann E, Weber A, Wilson LC, Douglas AGL, McGowan R, Need A, Bond A, Tavares ALT, Thomas ERA, Hill SL, Deans ZC, Boardman-Pretty F, Caulfield M, Scott RH, Wilkie AOM, Genomics England Research Consortium. Evaluating the performance of a clinical genome sequencing program for diagnosis of rare genetic disease, seen through the lens of craniosynostosis. *Genet Med* 2021;23:2360–8.
14 Karczewski KJ, Francioli LC, Tiao G, Cummings BB, Alföldi J, Wang Q, Collins RL, Laricchia KM, Ganna A, Birnbaum DP, Gauthier LD, Brand H, Solomonson M, Watts NA, Rhodes D, Singer-Berk M, England EM, Seaby EG, Kosmicki JA, Walters RK, Tashman K, Farjoun Y, Banks E, Poterba T, Wang A, Seed C, Whiffin N, Chong JX, Samocha KE, Pierce-Hoffman E, Zappala Z, O'Donnell-Luria AH, Minikel EV, Weisburd B, Lek M, Ware JS, Vittal C, Armean IM, Bergelson L, Cibulskis K, Connolly KM, Covarrubias M, Donnelly S, Ferriera S, Gabriel S, Gentry J, Gupta N, Jeandet T, Kaplan D, Llanwarne C, Munshi R, Novod S, Petrillo N, Roazen D, Ruano-Rubio V, Saltzman A, Schleicher M, Soto J, Tibbetts K, Tolonen C, Wade G, Talkowski ME, Neale BM, Daly MJ, MacArthur DG, Genome Aggregation Database Consortium. The mutational constraint spectrum quantified from variation in 141,456 humans. *Nature* 2020;581:434–43.
15 Lindeboom RGH, Vermeulen M, Lehner B, Supek F. The impact of nonsense-mediated mRNA decay on genetic disease, gene editing and cancer immunotherapy. *Nat Genet* 2019;51:1645–51.
16 Zhang J, Wright KD, Mahoney Rogers AA, Barrett MM, Shim K. Compensatory regulation of the size of the inner ear in response to excess induction of otic progenitors by fibroblast growth factor signaling. *Dev Dyn* 2014;243:1317–27.
17 Wright KD, Mahoney Rogers AA, Zhang J, Shim K. Cooperative and independent functions of FGF and Wnt signaling during early inner ear development. *BMC Dev Biol* 2015;15:15–33.
18 Twigg SRF, Wilkie AOM. A genetic-pathophysiological framework for craniosynostosis. *Am J Hum Genet* 2015;97:359–77.
19 Timberlake AT, Furey CG, Choi J, Nelson-Williams C, Loring E, Galm A, Kahle KT, Steinbacher DM, Larysz D, Persing JA, Lifton RP, Yale Center for Genome Analysis. De novo mutations in inhibitors of Wnt, BMP, and Ras/ERK signaling pathways in non-syndromic midline craniosynostosis. *Proc Natl Acad Sci U S A* 2017;114:E7341–7.
20 Chen P-C, Yin J, Yu H-W, Yuan T, Fernandez M, Yung CK, Trinh QM, Peltekova VD, Reid JG, Tworog-Dube E, Morgan MB, Muzny DM, Stein L, McPherson JD, Roberts AE, Gibbs RA, Neel BG, Kucherlapati R, . Next-Generation sequencing identifies rare variants associated with Noonan syndrome. *Proc Natl Acad Sci U S A* 2014;111:11473–8.

Craniosynostosis, inner ear, and renal anomalies in a child with complete loss of *SPRY1* (sprouty homolog 1) function

Tooze RS, Calpena E, *et al.*

Supplemental Methods

Analysis of whole genome sequencing data

Variants were annotated with Ensembl Variant Effect Predictor[1] and a Combined Annotation Dependent Depletion (CADD)[2] score to determine the consequence and predicted pathogenicity for each variant.

Lymphoblastoid Cell Culture

Blood (1.3 ml) was mixed with an equal volume of Phosphate Buffered Saline (PBS) and added to 3 ml of Sigma Histopaque®–1077 before centrifugation at 580 x *g* for 20 min at room temperature (RT). Peripheral blood mononuclear cells (PBMCs) were collected, PBS washed, and centrifuged (RT, 350 *g*, 5 min). The supernatant was discarded, and the cell pellet washed again in PBS (RT, 180 *g*, 5 min). Epstein-Barr virus (EBV, B95-9) was added to the PBMCs and incubated at 37°C for 1.5 hours. Cells were added to phytohemagglutinin M-form (Gibco, 10576-015) and maintained in culture medium (RPMI Medium 1648 (1x) supplemented with 15% Fetal Bovine Serum (FBS; Gibco, 10082-147), 1X penicillin-streptomycin (Gibco, 15140-122) and 1X L-glutamine (Gibco, 25030-081), incubated at 37°C, 5% CO_2.

RNA extraction and cDNA synthesis

Lymphoblastoid cells were cultured and harvested by centrifugation. RNA was extracted from cell pellets using the RNeasy Mini Kit (Roche) following the manufacturer's protocol. *DNase I* (5 µl of 1U/ µl, (Sigma-Aldrich, AMPD1)) was added to 5 µl of reaction buffer (R6273) and 50 µl of eluted RNA and incubated at RT for 15 min. Stop Solution (1 µl of 50 mM EDTA) was added to DNase-treated RNA and incubated at 70°C for 10 min, before reverse transcription (RevertAid First Strand cDNA Synthesis Kit (ThermoScientific, #K1622)).

Tooze RS, *et al. J Med Genet* 2022;0:1–5. doi: 10.1136/jmg-2022-108946

Polymerase chain reaction (PCR) of cDNA

A 2 μl sample of cDNA was diluted in a master mix containing 5 μl 5X Q5 reaction buffer, 1.25 μl each of 10 μM forward and reverse primer, 0.5 μl of dNTPs (10 mM), 5 μl of 5X Q5 GC enhancer, 0.25 μl of Q5 high fidelity enzyme and up to 25 μl of water. Samples were placed in the thermocycler under the following conditions: 98°C for 30 s, followed by 35 cycles of 98°C for 10 s, 70°C for 20 s, 72°C for 30 s, and a final elongation of 72°C for 2 min. Samples underwent dideoxy sequencing by the MRC Weatherall Institute of Molecular Medicine sequencing facility.

Next Generation Sequencing (MiSeq)

A 50ng sample of each cDNA sample was mixed with 4 μl 5X Q5 buffer, 1 μl each of 10 μM forward and reverse primer, 0.4 μl of dNTPs (10 mM), 0.2 μl of Q5 high fidelity enzyme and up to 20 μl of water. The sample was placed in the thermocycler under the following conditions: 98°C for 30 sec, followed by 30 cycles of 98°C for 10 sec, 70°C for 30 sec, 72°C for 30 sec, and a final elongation of 72°C for 8 min. The PCR product was diluted 100x and mixed with a 2 μl sample of CS barcode (2 μM, Fluidigm Access Array Barcode Library for Illumina Sequencer 100-4876) diluted in 5 μl of iProof high-fidelity master mix (BIO-RAD, 1725310) and 2 μl of nuclease-free water. Barcodes were annealed to the sample under the following conditions: 98°C for 2 min, followed by 8 cycles of 98°C for 10 sec, 60°C for 30 sec, 72°C for 30 sec and a final elongation of 72°C for 2 min. The final product was gel purified, diluted, and sequenced using a Miseq Reagent Kit v2 by the WIMM sequencing facility.

Western blot (WB)

Lymphoblastoid cells were incubated with fresh media 24 hours prior to harvest by centrifugation (300 *g*, 5 min). Lysis buffer (50 μL, Cellytic M lysis buffer (Sigma-Aldrich) containing proteases (Complete, Sigma-Aldrich) and phosphatase (PhosStop, Sigma-Aldrich) inhibitors) was added to each sample and left on ice for 30 min. The lysed samples were centrifuged at 18,000 *g* for 15 min at 4°C and the supernatant collected. Total protein concentration was quantified using a BCA Quantification Kit (ThermoScientific, 23225) and absorbance read at 562 nm (Spectra Max M2E). Samples were loaded onto polyacrylamide gels (4–20% Mini-PROTEAN® TGX™ Precast Gels, #4561094, BIO-RAD), containing 25 μg

protein sample, 6x loading dye and nuclease-free water. Samples were run for 1.5 hours at 120 V in 1x Tris-Glycine-SDS buffer before being transferred to a membrane (Immobilion®-hydrophilic polyvinylidene fluroride membrane) for 1 hour at 100 V. The membrane was blocked with 5% non-fat, blotting-grade milk (Bio-Rad) and left shaking gently for 1 hour at RT. Anti-Spry-1 (rabbit mAb D9V6P #13013, Cell Signaling Technology) diluted 1:1000 was added to the membrane and left shaking at 4^{o}C overnight, before washing with Tween Tris-buffered saline and adding secondary donkey anti-rabbit-HRP (abcam, ab97085) for 1 hour at RT, shaking gently. SuperSignal West Pico Plus Chemiluminescent Substrate Kit (Thermo Scientific) was used to develop the signal for 5 min before imaging. The primary and secondary antibodies were removed using the restore western blot stripping buffer (Thermo Scientific) before being stained with anti-GAPDH-HRP (14C10, Cell Signaling Technology) diluted 1:10,000 at RT for 1.5 hours.

Targeted resequencing

Analysis of 617 samples with undiagnosed craniosynostosis was undertaken using IDT's hybridisation and capture protocol. DNA samples were fragmented following the Swift 2S^{TM} Turbo v2 DNA Library Kit protocol and analysed using broad-range Qubit and D1000 TapeStation reagents, ensuring an average fragment size of 330bp. The prepared libraries were pooled to a total of 6 μg of DNA and up to 40 samples per hybridisation capture reaction. The hybridisation reactions were carried out at 65^{o}C for 16 hours. After hybridisation, the pooled libraries were washed and post-capture PCR was performed, following manufacturer's protocol (IDT xGen hybridization capture of DNA libraries for NGS target enrichment) for a panel containing 2054 probes. The amplified capture reactions were washed with beads and quantified and validated using high-sensitivity (HS) qubit reagents and HS D1000 TapeStation before next generation sequencing analysis using Miseq. Variants were analyses using amplimap software.[3]

Supplemental Table 1: List of primers

Primer Name	Sequence (5'-3')	Length	Tm	GC%	Assay
SPRY1_Leu27_F	TGCCAGGTTTCCACTGATT	19	57	47	Sanger Sequencing
SPRY1_1R	GTGTGTCTGTGCTCGTAGTT	20	57	50.0	Sanger Sequencing
SPRY1_Ex2-3_Junc_F	GAAAAGGGATTTCAGATGCATGCCAGG	27	60	48	RT-PCR
SPRY1_Ex3_R	CATGCTTTTCTTGTCTTGGTGCTGTC	26	61	46	RT-PCR
SPRY1_Ex3_CS_FW	ACACTGACGACATGGTTCTAACAGAA AAGGGATTTCAGATGCATGCCAGG	51	68.2	45	NGS
SPRY1_Ex3_CS_RV	TACGGTAGCAGAGACTTGGTCTCATG CTTTTCTTGTCTTGGTGCTGTC	48	68	48	NGS

Supplemental Table 2: Coordinates of the capture probes used in the targeted resequencing analysis

Chromosome	Start	End	Probe ID
chr4	123401501	123401621	788227_47098358_Target303_SPRY1_ENST00000610581.4_1
chr4	123401561	123401681	788227_47098358_Target303_SPRY1_ENST00000610581.4_2
chr4	123401621	123401741	788227_47098358_Target303_SPRY1_ENST00000610581.4_3
chr4	123401681	123401801	788227_47098358_Target303_SPRY1_ENST00000610581.4_4
chr4	123401741	123401861	788227_47098358_Target303_SPRY1_ENST00000610581.4_5
chr4	123401801	123401921	788227_47098358_Target303_SPRY1_ENST00000610581.4_6
chr4	123401861	123401981	788227_47098358_Target303_SPRY1_ENST00000610581.4_7
chr4	123401921	123402041	788227_47098358_Target303_SPRY1_ENST00000610581.4_8
chr4	123401981	123402101	788227_47098358_Target303_SPRY1_ENST00000610581.4_9
chr4	123402041	123402161	788227_47098358_Target303_SPRY1_ENST00000610581.4_10
chr4	123402101	123402221	788227_47098358_Target303_SPRY1_ENST00000610581.4_11
chr4	123402161	123402281	788227_47098358_Target303_SPRY1_ENST00000610581.4_12
chr4	123402221	123402341	788227_47098358_Target303_SPRY1_ENST00000610581.4_13
chr4	123402281	123402401	788227_47098358_Target303_SPRY1_ENST00000610581.4_14
chr4	123402341	123402461	788227_47098358_Target303_SPRY1_ENST00000610581.4_15
chr4	123402401	123402521	788227_47098358_Target303_SPRY1_ENST00000610581.4_16
chr4	123402461	123402581	788227_47098358_Target303_SPRY1_ENST00000610581.4_17
chr4	123402521	123402641	788227_47098358_Target303_SPRY1_ENST00000610581.4_18

Supplemental Table 3: Variants identified after filtering by allele frequency and CADD score

Gene	Chr	Pos[a]	Nucleotide and amino acid change	Mode of inheritance	Allele Frequency (AF)[b]	dbSNP	CADD score (PHRED)	Reported Phenotypes	Reason discounted
CCDC80	3	112609989	NM_199511.2: c.2414C>T; p.(Ala805Val)	Recessive	0.008783	rs56683778	31	Colorectal carcinoma	60 reported homozygous A805V variants in gnomAD V2.1.1
RASSF6	4	73587902	NM_177532.5: c.320A>G; p.(Tyr107Cys)	Recessive	-	rs776608439	25.5	Multiple cancers	Multiple amino acids tolerated at this position.
SPRY1	4	123401671	NM_001258038.2: c.80T>A; p.(Leu27*)	Recessive	-	-	35	Craniofacial malformation Kidney and urinary tract malformation	-
POMP	13	28664562	NM_015932.6: c.155A>G; p.(Glut52Gly)	*De novo*	-	-	31	Keratosis linearis with ichthyosis congenita and sclerosing keratoderma; proteasome-associated autoinflammatory syndrome 2	Associated disorders arise from indels. Described phenotypes are not consistent with our patient.[4]
ATXN10	22	45700287	NM_013236.4: c.397C>T; p.(Arg133Cys)	*De novo*	0.000024	-	28.1	Spinocerebellar ataxia	6 other reported heterozygous variants in gnomAD. Atxn10 heterozygous mice show no overt phenotype.[5]

[a]Genome GRCh38
[b]gnomAD AF taken from V2.1.1 (combined exome and genome data). AF for *de novo* variants was set at below 0.001, whereas AF for recessive variants was set at less than 0.01.

Supplemental Table 4: Deep sequencing of cDNA from both parents and the affected child

Family Member	Reference Allele	Alternative Allele
Mother	6126/12692 = 48%	6565/12692 = 52%
Father	11841/22180 = 53%	10337/22180 = 47%
Proband	5/21937 = 0.02%	21930/21937 = 100%

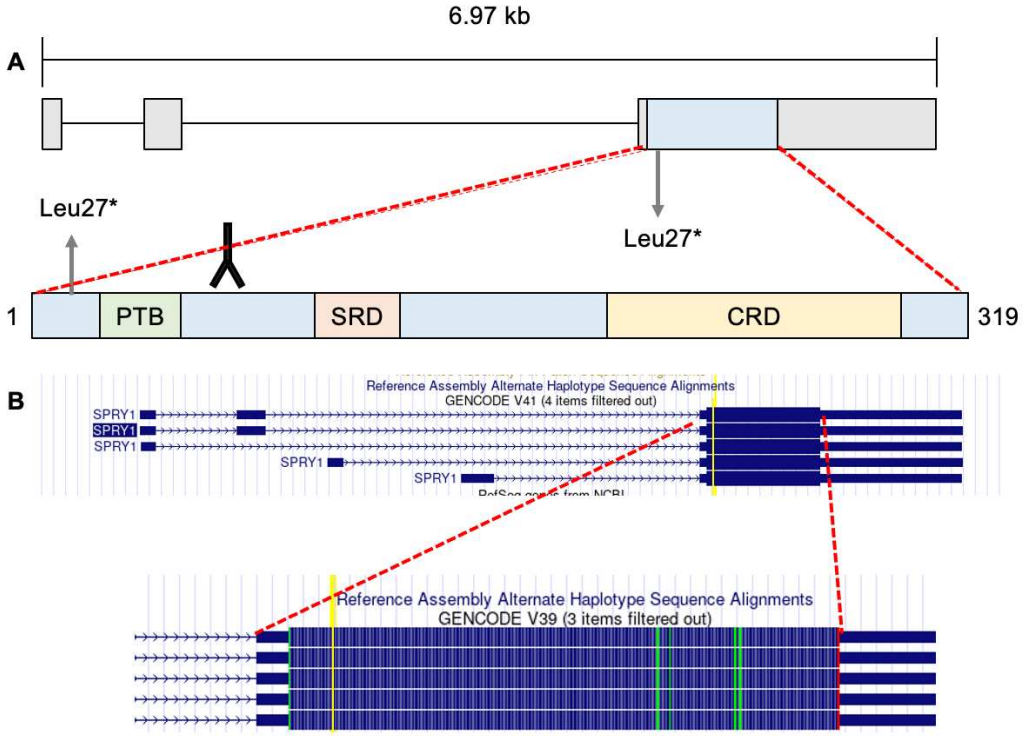

Supplemental Figure 1: *SPRY1* exon structure and predicted consequence of p.(Leu27)* nonsense variant. (A) Schematic of *SPRY1* with the coding region marked in blue and the non-coding exons in grey. Below, encoded protein showing conserved domains (PTB, phosphotyrosine-binding domain; SRD, serine-rich domain; CTD, cysteine-rich domain). The position of the antibody in the translated protein is indicated (inverted Y). (B) Screenshot from the UCSC web browser (https://genome.ucsc.edu/) showing that all transcripts of *SPRY1* would be affected by the p.(Leu27*) variant (position marked by the yellow line). Below, the coding exon has been zoomed in to identify any further methionine residues (highlighted in green), which all reside downstream of p.(Leu27).

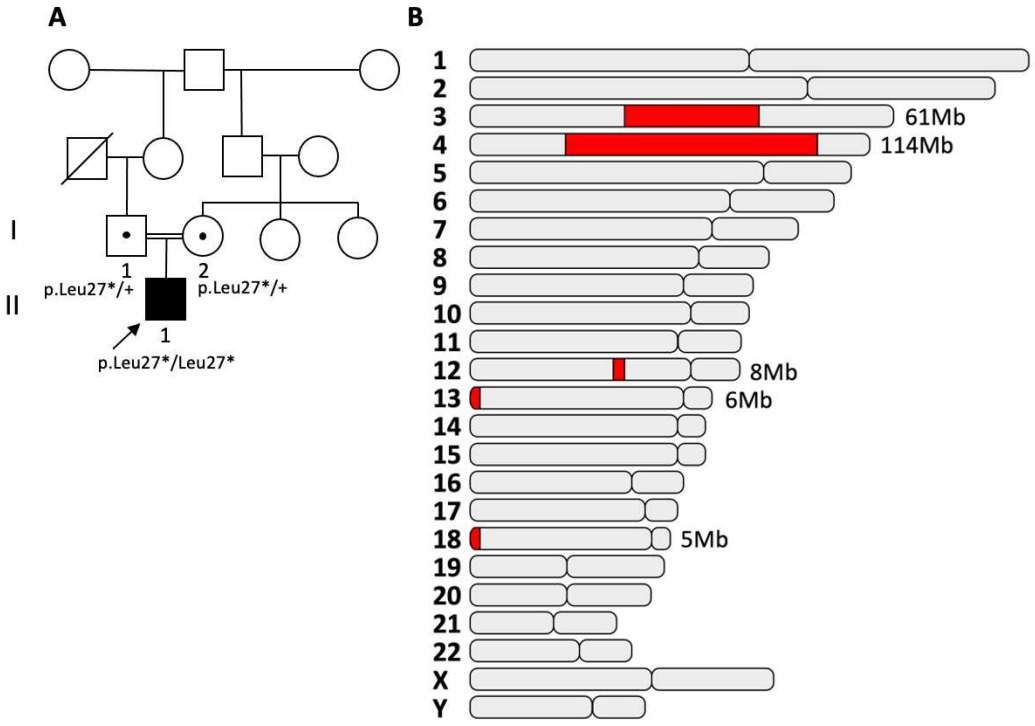

Supplemental Figure 2: Family pedigree and homozygosity analysis of WGS data from the proband II-1. (A) Pedigree figure illustrating both heterozygous parents with known consanguinity and the index patient, homozygous for p.(Leu27*) in SPRY1. (B) The output from ROHcaller is depicted in a schematic showing each chromosome, with regions of homozygosity larger than 2 Mb highlighted in red. *SPRY1* resides within the largest region of homozygosity (114 Mb) located on chromosome 4.

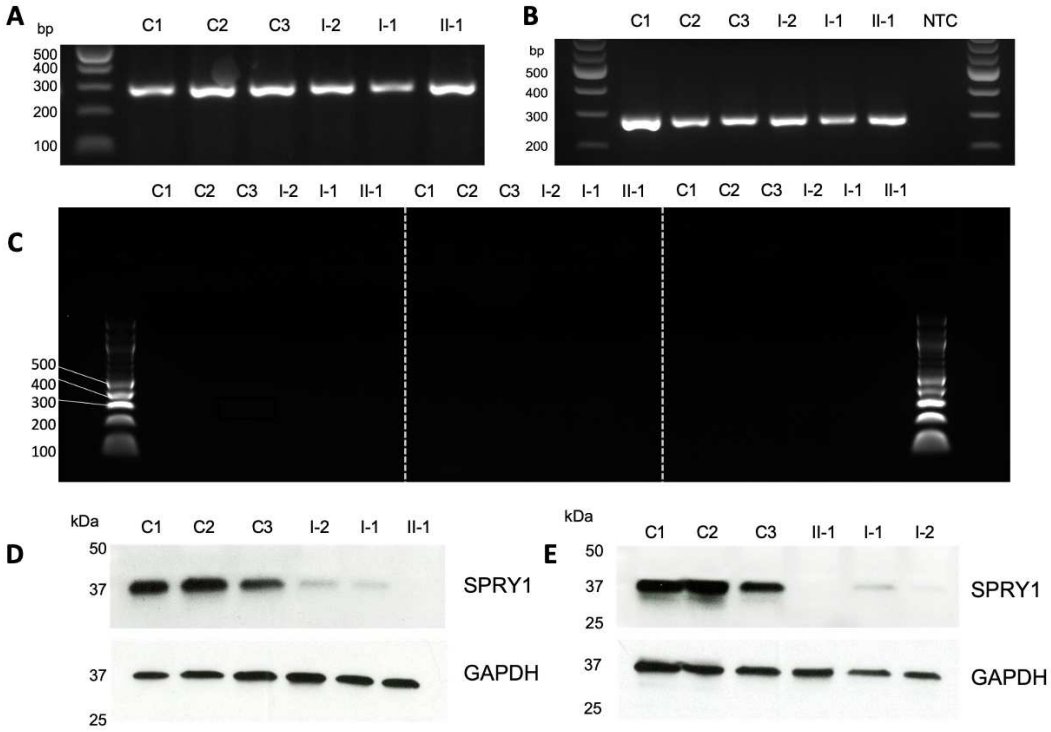

Supplemental Figure 3: Additional replicates of functional studies. (A-B) Two additional biological replicates of the RT-PCR including a negative no-template control (NTC). C1-3 = control 1-3, I-2 = mother, I-1 = father, II-1 = proband. (C) All no reverse-transcriptase controls (24 samples, including three repeats of C1-3, I-1, I-2, and II-1) were amplified using *SPRY1* primers and run on a 2% ethidium bromide gel. (D-E) Two further repeats of the western blot analysis alternating sample position.

REFERENCES

1. McLaren W, Gil L, Hunt SE, et al. The Ensembl Variant Effect Predictor. *Genome Biol* 2016;17(1):122.
2. Rentzsch P, Witten D, Cooper GM, et al. CADD: predicting the deleteriousness of variants throughout the human genome. *Nucleic Acids Res* 2019;47(D1):D886-D94.
3. Koelling N, Bernkopf M, Calpena E, et al. Amplimap: a versatile tool to process and analyze targeted NGS data. *Bioinformatics* 2019;35(24):5349-50.
4. Poli MC, Ebstein F, Nicholas SK, et al. Heterozygous Truncating Variants in POMP Escape Nonsense-Mediated Decay and Cause a Unique Immune Dysregulatory Syndrome. *Am J Hum Genet* 2018;102(6):1126-42.
5. Wakamiya M, Matsuura T, Liu Y, et al. The role of ataxin 10 in the pathogenesis of spinocerebellar ataxia type 10. *Neurology* 2006;67:607-13.